Effect of angular momentum on equilibrium properties of a self-gravitating system

Olivier Fliegans* and D. H. E. Gross
Hahn-Meitner-Institut Berlin, Bereich Theoretische Physik (SF5), Glienickerstrasse 100, D-14109 Berlin, Germany
(Received 4 February 2001; published 11 April 2002)

The microcanonical properties of a two-dimensional system of N classical particles interacting via a smoothed Newtonian potential, as a function of the total energy E and the total angular momentum L, are discussed. The two first moments of the distribution of the linear momentum of a given particle at a fixed position show that (a) on average the system rotates like a solid body and (b) the velocity dispersion is a function of the distance from the center. In order to estimate suitable observables, a numerical method based on an importance sampling algorithm is presented. The entropy surface S shows a negative specific heat capacity region at fixed L for all L. Observables probing the average mass distribution are used to understand the link between thermostatistical properties and the spatial distribution of particles. In order to define a phase in a nonextensive system, we introduce a more general observable than that proposed by Gross and Votyakov [Eur. Phys. J. B **15**, 115 (2000)]. This observable is the sign of the largest eigenvalue of the Hessian matrix of the entropy surface. If it is negative then the system is in a pure (single) phase; if it is positive then the system undergoes a first order phase transition. At large E the gravitational system is in a homogeneous gas phase. At low E there are several collapse phases. At $L=0$ there is a single-cluster phase and for $L\neq 0$ there are several phases with two clusters. The relative size of the clusters depends on L. All these pure phases are separated by a first order phase transition region. Signals of critical behavior emerge at several points of the parameter space (E,L). We also show that a huge loss of information appears if we treat the system as a function of the intensive parameters. Besides the known nonequivalence at first order phase transitions, the pure phases with two clusters of different sizes are not accessible to the canonical ensemble. Moreover, for a particular choice of intensive parameters introduced in this paper, there exist in the microcanonical ensemble some values of those intensive parameters for which the corresponding canonical ensemble *does not exist*, i.e., the partition sum *diverges.*

DOI: 10.1103/PhysRevE.65.046143 PACS number(s): 05.70.Fh, 05.20.Gg, 05.10.Ln

I. INTRODUCTION

The thermostatistical properties of systems of N classical particles under a long-range attractive potential have been extensively studied since the seminal work of Antonov [1–7]. One of their more specific and interesting properties is that they are unstable for all N [2] and, therefore, not thermodynamically extensive, i.e., they exhibit negative specific heat capacity regions even when the system is composed by a very large number of particles.

It is quite natural to ask whether the total angular momentum L, which is an integral of motion for systems of relevance in astrophysical context, plays a nontrivial role on the equilibrium properties of these systems. Indeed L is considered as an important parameter in order to understand the physics of systems such as galaxies [8–10], globular clusters [11–14], molecular clouds in the multifragmentation regime [15,16], which might eventually lead to stellar formation [17–22,25].

Previous works have already studied the effect of L in the mean field limit with a simplified potential and by imposing a spherical symmetry [26], or at $L=0$ [13]. Our work, presented in this paper, is an attempt to overcome some of these approximations.

Thermodynamical equilibrium does not exist for Newtonian self-gravitating systems, due both to evaporation of stars (the systems are not self-bounded) and short distance singularities in the interaction potential. However there exist intermediate stages where these two effects might be neglected and a quasiequilibrium state might be reached (dynamical issues like ergodicity, mixing, or ''approach to equilibrium'' [7,27,28] are not considered in this paper). In order to make the existence of equilibrium configurations possible we have, first, to bound the system in an artificial box and, second, to add a short distance cutoff to the potential. The latter point can be seen as an attempt to take into account the appearance of new physics at very short distances (about the influence of this short distance cutoff see [29–31]). Another way to avoid the difficulties due to the short distance singularity is to describe the function of distribution of the ''stars'' within Fermi-Dirac statistics [3,32].

The box breaks the translational symmetry of the system; therefore the total linear momentum P and angular momentum with respect to the center of mass of the system L are not conserved. Nevertheless we assume that the equilibration time is smaller than the characteristic time after which the box plays a significant role [13,26]. Therefore P and L are considered as (quasi-) conserved quantities. We put the center of the box at the center of mass R_{CM}, which is also set to be the center of the coordinates. Therefore $P=0$.

As already mentioned, self-gravitating systems are nonextensive and a statistical description based on their intensive parameters (canonical ensemble) should be taken with caution since the different statistical ensembles are only equivalent at the thermodynamical limit far from first order transi-

*Corresponding author. Email address: fliegans@rhrk.uni-kl.de

tions (see Sec. III D). Moreover, this limit, which is not defined for self-gravitating systems, is required in order to define phases and phase transitions if one fixes the intensive parameters [33]. In contrast, the microcanonical ensemble (ME) does not require this limit and allows a classification of phase transitions for finite-size systems [34,35]. Hence the considered system is studied within the natural ME framework.

In order to perform the computation in a reasonable time we have to consider a two-dimensional system.

The paper is organized as follows. In Sec. II we recall the analytical expressions for entropy and its derivatives (Sec. II A), generalize the definition of phase transitions for nonextensive systems proposed in [34] (Sec. II B), discuss the two first moments of the distribution of the linear momentum of a given particle at a fixed position (Sec. II C), and present a numerical method based on an importance sampling algorithm in order to estimate suitable observables (Sec. II D). Numerical results are presented in Sec. III; the link between the average mass distribution and the thermostatistical properties is made in Sec. III B. In Sec. III C we use the definition of phase introduced in Sec. II B to draw the phase diagram of the self-gravitating system as a function of its energy E and angular momentum L. Finally, we introduce a nonstandard canonical ensemble (GBE). This ensemble is a function of the (intensive) variables conjugate of E and L^2. It is inspired from another nonstandard canonical ensemble introduced in [23], see [24]. We discuss the results obtained from GBE and also from the standard canonical ensemble. For our model we show how the predictions using these ensembles are inaccurate and misleading (Sec. III D). Results are summarized and discussed in Sec. IV.

II. MICROCANONICAL PROPERTIES

A. Microcanonical definitions

Consider a system of N classical particles on a disk of radius R whose interaction is described by a Plummer softened potential [36,37]

$$\varphi_{ij} = -\frac{Gm_i m_j}{\sqrt{s^2+(\boldsymbol{q}_i-\boldsymbol{q}_j)^2}}, \tag{1}$$

where m_i and $\boldsymbol{q}_i=\{q_i^1,q_i^2\}$ are the mass and position of particle i, respectively, s is the softening length, and G is the gravitational constant. The fixed total energy E is described by the Hamiltonian

$$\mathcal{H}=\sum_i \frac{\boldsymbol{p}_i^2}{2m_i}+\varphi(\boldsymbol{q}), \tag{2}$$

where $\boldsymbol{p}_i=\{p_i^1,p_i^2\}$ is the linear momentum of particle i, $\varphi=\Sigma_{i<j}\varphi_{ij}$, $\boldsymbol{q}$ is a $2N$-dimensional vector whose coordinates are $\{\boldsymbol{q}_1,\ldots,\boldsymbol{q}_N\}$ representing the spatial configuration. $\mathbf{q}$ is an element of the spatial configuration space V_c, $\boldsymbol{q}\in V_c\subset\mathbb{R}^{2N}$.

The entropy S is given through the Boltzmann's principle (the Boltzmann constant is set to 1),

$$S(E,L,N)=\ln[W(E,L,N)], \tag{3}$$

where $W(E,L,N)$ is the volume of the accessible phase space with E, L, and N fixed (under the assumptions given in Sec. I)

$$W(E,L,N)=\frac{1}{N!}\int\prod_{i=1}^{N}\left(\frac{d\boldsymbol{p}_i d\boldsymbol{q}_i}{(2\pi\hbar)^2}\right)\delta(E-\mathcal{H})\,\delta^{(2)}\left(\sum_i \boldsymbol{p}_i\right)\times\delta\left(L-\sum_i \boldsymbol{q}_i\times\boldsymbol{p}_i\right)\delta^{(2)}\left(\sum_i \boldsymbol{q}_i\right), \tag{4}$$

where $\boldsymbol{q}_i\times\boldsymbol{p}_i=q_i^1p_i^2-q_i^2p_i^1$. After integration over the momenta, Eq. (4) becomes [26,38]

$$W(E,L,N)=\mathcal{C}\int_{V_c}d\boldsymbol{q}\frac{1}{\sqrt{I}}E_r^{N-5/2}, \tag{5}$$

where

$$\mathcal{C}=\frac{(2\pi)^{(N-3/2)}\prod_i m_i}{(2\pi\hbar)^{2N}N!\left(\sum_i m_i\right)\Gamma(N-3/2)}$$

is a constant, $I=\Sigma_i m_i\boldsymbol{q}_i^2$ is the inertial momentum, and $E_r=E-L^2/2I-\varphi$ is the remaining energy. From the point of view of the remaining energy, if $L\neq 0$ we can already notice that the equilibrium properties are the results of a competition between two terms; the rotational energy $L^2/2I$ and the potential energy φ. The former tries to drive the particles away from the center of mass in order to increase I whereas the latter tries to group the particles together in order to decrease φ, but since the center of mass is fixed this will lead to a concentration of particles near the center and consequently will decrease I.

The microcanonical temperature T is defined by

$$\frac{1}{T}=\beta\equiv\frac{\partial S}{\partial E}=\left\langle\frac{N-5/2}{E_r}\right\rangle, \tag{6}$$

where $\langle\cdot\rangle$ is the microcanonical average

$$\langle\mathcal{O}\rangle=\frac{\mathcal{C}}{W}\int_{Vc}d\boldsymbol{r}\frac{\mathcal{O}(\boldsymbol{r})}{\sqrt{I}}E_r^{N-5/2}. \tag{7}$$

The angular velocity ω is defined as the negative of the conjugate force of L times T [39],

$$\omega\equiv-\frac{1}{\beta}\frac{\partial S}{\partial L}=\frac{\left\langle\frac{L}{I}E_r^{-1}\right\rangle}{\langle E_r^{-1}\rangle}. \tag{8}$$

We also define $\gamma\beta$ as the conjugate forc of L^2,

$$\gamma\beta \equiv \frac{\partial S}{\partial L^2} = -\left\langle \frac{1}{2I}\frac{N-5/2}{E_r}\right\rangle, \tag{9}$$

$$\omega = -2L\gamma. \tag{10}$$

B. Phase and phase transitions

For finite-size systems or self-gravitating systems phase transitions cannot be defined in the usual way, e.g., by means of Lee and Yang singularities [33], since these singularities show up only at the thermodynamical limit. Invoking the thermodynamical limit when studying finite-size systems washes out all the finite-size effects that may lead to new phenomena, (e.g., isomerization of metallic clusters [40], multifragmentation of nuclei [41]) and for self-gravitating systems the thermodynamical limit does not exist. Hereafter, a system will be considered as ''Small'' if the range of the forces is of the order of the system size (e.g., metallic clusters, nuclei, and self-gravitating systems) and also if the system has no proper thermodynamical limit (e.g., unstable systems [42] and also self-gravitating systems).

In a recent paper [34] definitions of pure (single) phases and phase transitions (first and second kind) based on the *local* topology of the microcanonical entropy surface have been proposed. In the following we first fix some notations and then recall the definitions.

Consider the ME of an isolated physical system. Its associated entropy $S(X)$ is a function of $\mathcal{M}$ ''extensive'' dynamical conserved quantities $X=\{X^1,\ldots,X^{\mathcal{M}}\}$. Note that X may not contain *all* the dynamical conserved quantities and for simplicity all these parameters are considered as being continuous. The Hessian matrix of $S(X=X_0)$ is noted by $H_S(X_0)=\|\partial^2 S/\partial X^i \partial X^j\|_{X_0}$, its eigenvalues are $\{\lambda_1,\cdots,\lambda_{\mathcal{M}}\}$, where $\lambda_1\geqslant\lambda_2\geqslant\ldots\geqslant\lambda_{\mathcal{M}}$ and the determinant of $H_S(X)$ is $D_S=\lambda_1,\ldots,\lambda_{\mathcal{M}}$.

In [34] phase transitions are defined ''*by the points and regions of non-negative curvature of the entropy surface* $[\cdots]$ *as a function of the mechanical quantities*.'' Therein the sign of D_S is put forward as a measure of the concavity of S (its negative curvature), so that at first order phase transition

$$\mathrm{sgn}(D_S)=\mathrm{sgn}[(-1)^{\mathcal{M}+1}]. \tag{11}$$

Though this condition is *necessary* it is not *sufficient* in the general case. In fact S is a nonconcave function at X_0 if

$$\lambda_1(X_0)\geqslant 0, \tag{12}$$

i.e., if at least one eigenvalue of H_S is non-negative. Note that in the two-dimensional sample model studied in [34] in order to illustrate the definition (11), λ_2 is always negative and therefore the sign of D_S is simply the opposite of that of λ_1, and the conditions (11) and (12) are equivalent.

Note that if $\mathcal{M}=1$ then $\lambda_1=\partial^2 S/\partial E^2\propto -C_v^{-1}$, where $C_v^{-1}\equiv \partial T(E)/\partial E$ is the microcanonical heat capacity. Hence, for $\mathcal{M}=1$, λ_1 and the heat capacity are of opposite sign.

By using $\mathrm{sgn}(\lambda_1)$, one can somewhat extend or clarify the classification of phase transitions for ''Small'' systems when the entropy is a function of $\mathcal{M}\geqslant 1$ variables.

(1) A single pure phase if $\lambda_1(X_0)<0$, i.e., if the entropy surface is locally concave at X_0. For $\mathcal{M}=1$ this corresponds to a *positive* heat capacity.

(2) A first order phase transition if $\lambda_1(X_0)>0$. For $\mathcal{M}=1$ this corresponds to a *negative* heat capacity. As mentioned in [34,43] the depth of the associated entropy intruder is a measure of the interphase surface tension in the case of systems with short-range interactions. How to define and measure these depths when $\mathcal{M}>1$ will be discussed elsewhere. Note that some eigenvalues might still be negative although $\lambda_1(X_0)>0$ just like in the model presented in [34]. In this case ''good'' order parameters are linear combinations of the eigenvectors whose eigenvalues are positive, see [44].

(3) If $\lambda_1(X_0)=0$ and λ_1 is the only zero eigenvalue, and $\nabla_{\mathbf{v}_1}\lambda_1=0$, where $\mathbf{v}_1$ is the eigenvector associated with λ_1, then there is a second order phase transition at X_0. For $\mathcal{M}=1$ this correspond to $\partial^2 S/\partial E^2=0$ and $\partial^3 S/\partial E^3=0$.

(4) If several eigenvalues obey $\lambda_i=0$ and $\boldsymbol{\nabla}_{\mathbf{v}_i}\lambda_i=0$ for $i=1,\ldots,n\leqslant\mathcal{M}$ then X_0 is a multicritical point.

C. Momentum average and dispersion

In this section we derive the average and the dispersion of the linear momentum of a particle, we also compute its mean angular velocity and relate it to that of the system as defined in Eq. (8).

The derivation of $\langle \boldsymbol{p}_k\rangle_{\boldsymbol{q}_k}$, the average momentum of particle k at fixed position $\boldsymbol{q}_k$ (while the other particles are free), is similar to that of W. Details of the derivation can be found in the Appendix and the result is

$$\langle \boldsymbol{p}_k\rangle_{\boldsymbol{q}_k} = L\langle I^{-1}\rangle_{\boldsymbol{q}_k} m_k \sum_{\alpha,\delta=1}^{2} \boldsymbol{\epsilon}_{\alpha\delta} q_k^{\delta}\hat{\mathbf{e}}_\alpha, \tag{13}$$

where $\boldsymbol{\epsilon}$ is the antisymmetric tensor of rank 2 and $\hat{\mathbf{e}}_\alpha$ is the unit vector of coordinate α. Equation (13) shows that $\langle \boldsymbol{p}_k\rangle_{\boldsymbol{q}_k}$ is a vector perpendicular to $\boldsymbol{q}_k$ whose module is a function of $\|\boldsymbol{q}_k\|$. In other words the orbit of a particle is, on an average, circular (this result is expected since the system is rotationally symmetric). One can compute $\langle \omega_k\rangle_{\boldsymbol{q}_k}$, the mean angular velocity of k at distance $\|\boldsymbol{q}_k\|$, by first considering $\langle L_k\rangle_{\boldsymbol{q}_k}$, the mean angular momentum of k at distance $\|\boldsymbol{q}_k\|$,

$$\langle L_k\rangle_{\boldsymbol{q}_k} \equiv \boldsymbol{q}_k \times \langle \boldsymbol{p}_k\rangle_{\boldsymbol{q}_k} = L\langle I^{-1}\rangle_{\boldsymbol{q}_k} I_k, \tag{14}$$

where $I_k=m_k\boldsymbol{q}_k^2$. The angular mean velocity of a particle on a circular orbit is classically linked to $\langle L_k\rangle_{\boldsymbol{q}_k}$ by

$$\langle L_k\rangle_{\boldsymbol{q}_k} = \langle \omega_k\rangle_{\boldsymbol{q}_k} I_k. \tag{15}$$

We can identify $\langle \omega_k\rangle_{\boldsymbol{q}_k}$ in Eq. (14) as

$$\langle \omega_k\rangle_{\boldsymbol{q}_k} = L\langle I^{-1}\rangle_{\boldsymbol{q}_k}. \tag{16}$$

The dependence of $\langle\omega\rangle_{q_k}$ on $||q_k||$ is of the order of $1/N$ [$\langle I^{-1}\rangle_{q_k}=\langle I^{-1}\rangle+O(N^{-1})$], therefore for large N we can write [see Eq. (8)]

$$\langle\omega_k\rangle_{q_k}\sim L\langle I^{-1}\rangle\approx\langle\omega\rangle. \tag{17}$$

For large N the mean angular velocity is the same for all the particles at any distance from the center; in other words, the system, on an average, rotates like a solid body. Moreover $\langle\omega_k\rangle_{q_k}$ corresponds to the thermostatistical angular velocity ω defined by Eq. (8). These are also classical results for extensive systems at low L [39,45]. Note also that these results do not depend on the interaction potential φ.

The momentum dispersion σ_{p_k} can also be derived. Using Eqs. (13) and (A5), we get for large N

$$\sigma^2_{p_k}\equiv\langle p_k^2\rangle_{q_k}-\langle p_k\rangle^2_{q_k}\sim 2\frac{m_k}{\beta}+I_kL^2m_k(\langle I^{-2}\rangle-\langle I^{-1}\rangle^2). \tag{18}$$

The second term of Eq. (18) is intensive and proportional to the square of the dispersion of I^{-1} and to q_k^2 ($I_k=m_kq_k^2$). When this term vanishes relative to the first one, e.g., when the fluctuations of I^{-1} are small, or at high energy (low β) and low L, we recover the usual dispersion of the Maxwell-Boltzmann distribution. This term also gives a correction to the usual equipartition theorem; for large N

$$\langle E_k\rangle\equiv\frac{\sigma^2_{p_k}}{2m_k}\sim T+\frac{I_kL^2}{2}(\langle I^{-2}\rangle-\langle I^{-1}\rangle^2), \tag{19}$$

where $\langle E_k\rangle$ is the average internal kinetic energy (without the contribution from the collective, hydrodynamical, rotational movement) of particle k. Again this correction is position-dependent via I_k. In regimes where the fluctuations of the mass distribution cannot be neglected in Eqs. (18) and (19), an estimation of the temperature based on the velocity dispersion would show that the temperature is smaller at the center than at the edge.

D. Numerical method

From now on we set $m_i=m\,\forall\ i=1,\ldots,N$ and use the following dimensionless variables: (i) $E\to\epsilon=ER/Gm^2N^2$; (ii) $L\to l^2=\Omega=L^2/2Gm^3RN^2$; (iii) $s\to\sigma=s/R$; (iv) $q\to r=q/R$; (v) $V_c\to v_c$; (vi) $\varphi\to\phi=(R/Gm^2N^2)\varphi=(-1/N^2)\Sigma_{i<j}1/\sqrt{\sigma^2+(r_i-r_j)^2}$; (vii) $I\to I=\Sigma_i r_i^2$. The weight (5) is now

$$W(\epsilon,\Omega)=\mathcal{C}'\int_{v_c}dr\,\frac{1}{\sqrt{I}}\epsilon_r^{N-5/2}, \tag{20}$$

where $\epsilon_r=\epsilon-\Omega/I-\phi$ is the dimensionless remaining energy and $\mathcal{C}'$ is a constant. Later on we no longer write this constant since it plays no significant role (it only shifts the entropy by $\ln\mathcal{C}'$). The derivatives of entropy (β, ω, ...) are now dimensionless.

One usually estimates Eq. (20) by means of some Monte Carlo algorithm, updating the positions $\mathbf{q}$ by some small amount $\delta\mathbf{q}$ in order to get a good pass acceptance, and using the configuration weight $W(r)=(1/\sqrt{I})\epsilon_r^{N-5/2}$ in the Metropolis pass. Unfortunately this strategy does not really work (within a reasonable CPU time), because the $2N$-dimensional configuration weight landscape at fixed ϵ and Ω presents troughs and high peaks [46]. Hence, exploring the total configuration space (or at least a subset containing the highest peaks) would take a very long, in practice infinite, time. This weight landscape looks like the energy landscape found in spin-glass systems.

The strategy we have adopted is described in the following. First we can rewrite Eq. (20) as

$$W(\epsilon,\Omega)=\int dId\phi D(I,\phi)\frac{1}{\sqrt{I}}\epsilon_r^{N-5/2}, \tag{21}$$

where $D(I,\phi)=\int_{v_c}dr\,\delta(I'(r)-I)\,\delta(\phi'(r)-\phi)$. $D(I,\phi)$ is the density of spatial configurations at given I and ϕ. Given D we can compute W, S, and its derivatives for *any* ϵ and Ω, e.g.,

$$\gamma=\frac{1}{\beta}\frac{\partial S}{\partial\Omega}=-\frac{N-5/2}{\beta}\frac{\int dId\phi D(I,\phi)I^{-3/2}\epsilon_r^{N-7/2}}{W(\epsilon,\Omega)}. \tag{22}$$

The expectation value $\langle\mathcal{O}\rangle$ of an observable $\mathcal{O}(r)$ can be estimated if we know D and $\langle\mathcal{O}\rangle_{I,\phi}$,

$$\langle\mathcal{O}\rangle\equiv\frac{\int_{v_c}dr\mathcal{O}(r)I^{-1/2}\epsilon_r^{N-5/2}}{\int_{v_c}drI^{-1/2}\epsilon_r^{N-5/2}}=\frac{\int dId\phi\langle\mathcal{O}\rangle_{I,\phi}D(I,\phi)I^{-1/2}\epsilon_r^{N-5/2}}{W(\epsilon,\Omega)}, \tag{23}$$

where

$$\langle\mathcal{O}\rangle_{I,\phi}=\frac{\int_{v_c}dr\mathcal{O}(r)\,\delta(I'-I)\,\delta(\phi'-\phi)}{D(I,\phi)}. \tag{24}$$

Now, we have to compute $D(I,\phi)$ and $\langle\mathcal{O}\rangle_{I,\phi}$. *A priori* $D(I,\phi)$ is highly peaked around the values of I and ϕ that describe the gas (disordered) phase and should drop down at the edges. Nevertheless in order to study the total parametric space (ϵ,l) a good estimate of $D(I,\phi)$ is needed for almost all values taken by (I,ϕ) even when $D(I,\phi)$ is very small compared to its maximum. For example, at small total energy ϵ only the part of $D(I,\phi)$ for which $\epsilon_r=\epsilon-l^2/I-\phi>0$ will contribute to the integral (21).

In order to get a good estimate of D we used an iterative scheme inspired by multicanonical algorithms [47–50]. The standard multicanonical task is to compute the free energy as

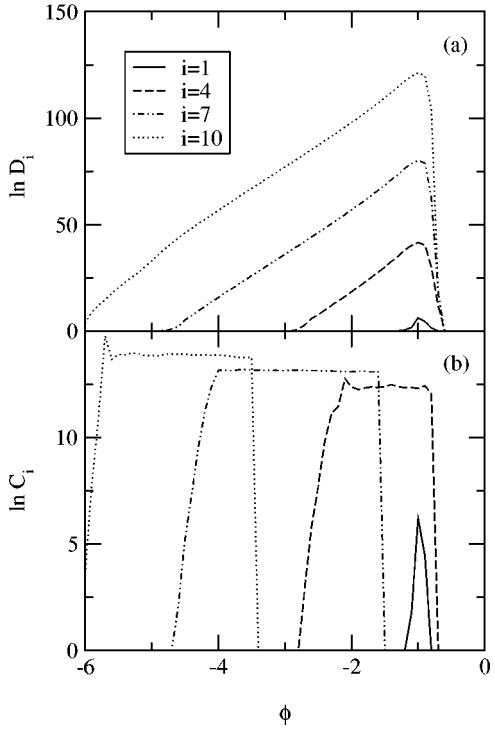

FIG. 1. Estimate of the density of state $D_i(I=3,\phi)$ (a) and histogram of the visited states $C_i(I=3,\phi)$ (b) at different iteration steps i of the multicanonical algorithm as a function of the potential energy ϕ and at fixed I. Panel (a) shows how D is built step by step; D is an extremely peaked function, the logarithm of the ratio between its maximum and its minimum is about 120. Without the blocking mechanism (see text) C_i would have been non-null for all values of ϕ visited during previous steps $j<i$. In panel (b) we see that the algorithm does no longer visit ''well-known'' regions ($\phi \gtrsim -1.5$) already after four steps.

a function of the total energy. Here we have to compute D as a function of I and ϕ. The updating scheme presented in [50] was used; one of the reasons for this choice is that although it has been given for a one-dimensional task it can be trivially extended to bivariate problems. Furthermore, we added a blocking mechanism: once we estimate that enough information has been collected on a given region of the parametric space (I,ϕ) then it is tagged as ''locked'' so that it will not be visited during the following iterations. This mechanism enables the program to spread more quickly over the parametric space and save computation time comparing to usual multicanonical algorithms. Details on this blocking mechanism are given elsewhere [44].

In the present paper we present results for $N=20$ and $\sigma=0.05$. Figure 1 shows a slice of $D(I,\phi)$ for $I=3$ at different iteration steps i [Fig. 1(a)]. We have also plotted the histogram $C(I=3,\phi)$ of the visited region in order to illustrate the blocking mechanism [Fig. 1(b)]. As expected D is strongly peaked around the disordered region $\phi \approx -1$ (this value corresponds to the mean of ϕ over randomly generated spatial configurations). After ten iterations the ratio between the maximum and the minimum of D is $\approx \exp(120)$. This ratio increases exponentially with N, e.g., at $N=10$ its value is $\approx \exp(80)$. This is the main reason why we could not study

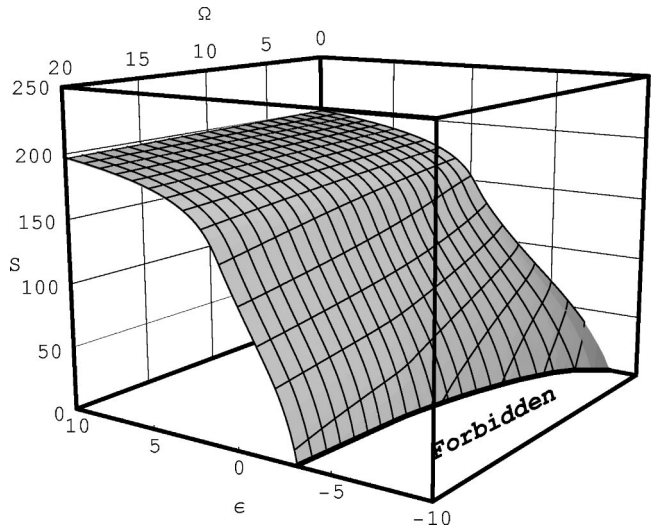

FIG. 2. Entropy surface $S(\epsilon,\Omega=l^2)$ (up to an arbitrary additional constant), the mesh lines are at constant ϵ or constant Ω. The thick line is close to the projection of the $T=0$ ($S\to-\infty$) isotherm. A convex intruder at constant Ω and for a certain energy range (e.g., $-2\lesssim\epsilon\lesssim 0$ for $\Omega=20$) can be seen for all Ω. S is not defined in the *forbidden region*, there the remaining energy ϵ_r is negative for all $\mathbf{q}\in v_c$.

systems with larger N within the current algorithm, but we should add that no qualitative changes have been noted between $N=10$ and $N=20$ (some preliminary studies support this remark for $N=50$). Work is in progress to overcome this limitation, though we are convinced that qualitatively the results presented in the following apply to systems with a larger number of particles.

III. RESULTS

A. Entropy and its derivatives

Figure 2 shows the entropy surface S as a function of ϵ and $\Omega=l^2$, the square of the unitless angular momentum l. The ground-state energy $\epsilon_g(\Omega)$ (thick line in Fig. 2) increases with Ω; ϵ_g classically corresponds to $\epsilon_r=0$ implying $S=-\infty$. For all Ω, $\epsilon_g(\Omega)$ is a concave function of Ω, i.e., $\partial^2\epsilon_g/\partial\Omega^2\leqslant 0$; at high Ω ($\Omega\gtrsim 12$) it is almost linear $\partial^2\epsilon_g/\partial\Omega^2\to 0^-$. These properties show that the set $\{\epsilon,\Omega\}$ over which S is defined is *not* convex [51], and in Sec. III D we discuss some consequences resulting from a nonconvex domain of definition.

At fixed Ω, $S(\epsilon)$ is not concave for all ϵ but shows for some energy interval a convex intruder, which signals a first order phase transition with negative specific heat capacity $(\partial\beta/\partial\epsilon>0)$ [35]. This can be better viewed by plotting $\beta(\epsilon,\Omega)=\partial S/\partial\epsilon$ (Fig. 3). Here the counter part of the entropy intruder is a region of multiple valued $\epsilon(\beta)$, this is the case for β between 15 and 20.

The latent heat at fixed Ω, $q_\epsilon(\Omega)$ decreases for $0\leqslant\Omega\lesssim 12$ and is a constant for $\Omega>12$. There is no critical value of Ω, Ω_c above which $S(\epsilon)$ is concave for all ϵ, i.e., there is a first order phase transition of all values of Ω. In another

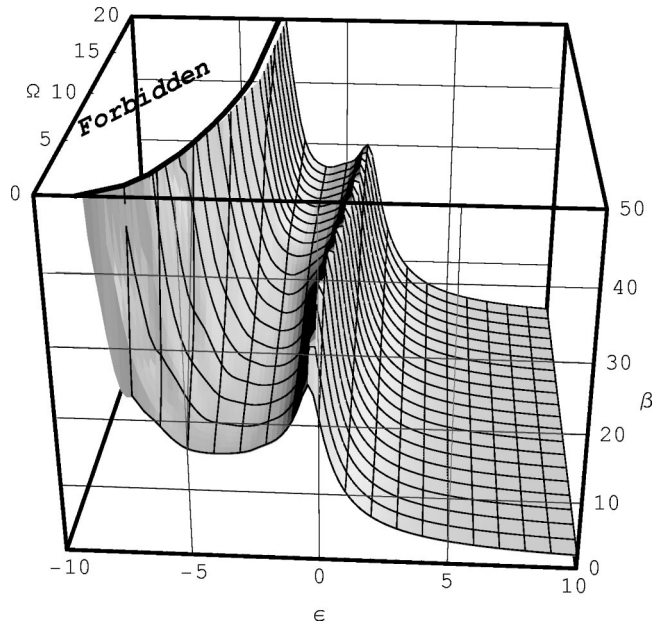

FIG. 3. Inverse temperature $\beta(\epsilon,\Omega=l^2)$ surface. The mesh lines are at constant ϵ or constant Ω. The intruder in S at fixed Ω corresponds here to a multiple energy value for a given β and Ω, e.g., $\beta(\epsilon,\Omega=0)=20$ has three solutions $\epsilon_1\approx 0$, $\epsilon_2\approx -1$, and $\epsilon_3 \approx -6$. The thick line is close to the projection of the $\beta=\infty$ isotherm; β is not defined in the *forbidden* region.

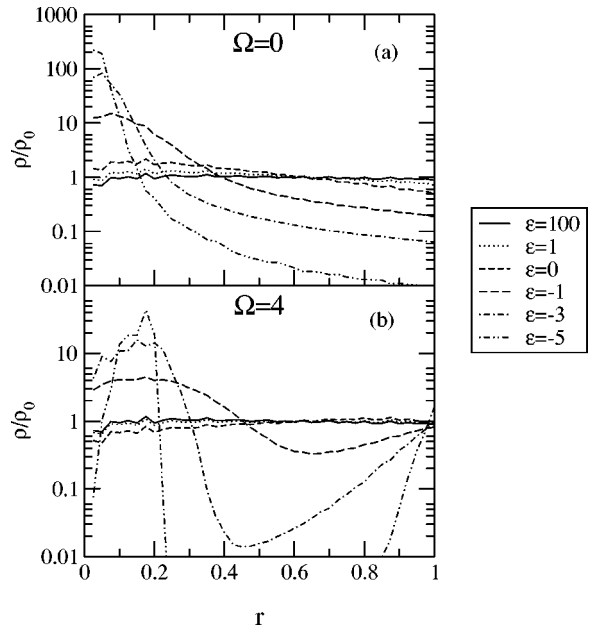

FIG. 5. Density ρ as a function of the distance from the center r at different values of energy ϵ and angular velocity Ω (arbitrary units). At high energy and for all Ω the density is flat; the system is in the homogeneous gas phase. Near the ground state the density shows one peak for $\Omega=0$ (a) and two peaks for $\Omega>0$ (b), which correspond, respectively, to a one-cluster and to a two-cluster phase surrounded by some gas (see text).

model for a self-gravitating system such a Ω_c was reported [26].

In Fig. 4 we have plotted the microcanonical angular velocity ω as a function of Ω and ϵ. As a direct consequence of Eq. (8) ω tends to zero with Ω, and at high energy ω is proportional to $\sqrt{\Omega}$ ($\propto l$). For low energies and $\Omega<12$, ω exhibits some structures with peaks and troughs, in other words at fixed ϵ, ω is not necessarily an increasing function of Ω. At high Ω ($\Omega>12$) and near the ground states ω is almost a constant. All these structures can be understood in terms of mass distributions, which influence ω through I (see Sec. III B).

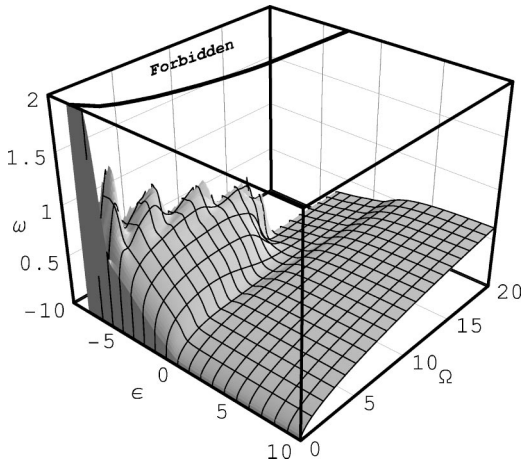

FIG. 4. Microcanonical angular velocity $\omega(\epsilon,\Omega=l^2)$ surface. The mesh lines are at constant ϵ or constant Ω. ω is not defined in the *forbidden* region. At high energy $\omega\propto\sqrt{\Omega}$; near the ground states ω shows a richer nonmonotonic behavior with peaks and troughs for small Ω and has a nearly constant value for large Ω (see text).

B. Mass distribution

In order to understand the origin of the structures seen in the different microcanonical quantities (S, β, ω, ...) we have to have a closer look at the spatial configurations, i.e., at the mass distributions. One observable we have studied is the mass density ρ [see Eqs. (23) and (24)]. As the Hamiltonian of the system is rotationally invariant, the mean value of ρ can only be a function of r, the distance from the center of coordinates, although other observables, e.g., two-body correlations might show a breaking of the rotational symmetry (see below).

On Fig. 5 ρ is plotted for different energies and for $\Omega=0$ and $\Omega=4$. For $\Omega=0$ [Fig. 5(a)] we recover the classical case (when E is the only fixed parameter). At high energy the system is in a homogeneous gas phase (flat ρ); when the energy decreases the system undergoes a phase transition and eventually ends up in a collapse phase where a majority of particles are in a cluster near the center of coordinates (ρ peaked at $r=0$). For $\Omega\neq 0$ [Fig. 5(b)] the situation is very different. At high energy we recover the homogeneous gas phase. But at low energy the system cannot collapse entirely at the center of mass. This is due to the rotational energy $\epsilon_{rot}=\Omega/I$ in Eq. (5). If the system contracts at the center, the inertial momentum I will tend to zero and, therefore, ϵ_{rot} will diverge leading to a negative remaining energy ϵ_r. So depending on the value of Ω the main cluster will eject a

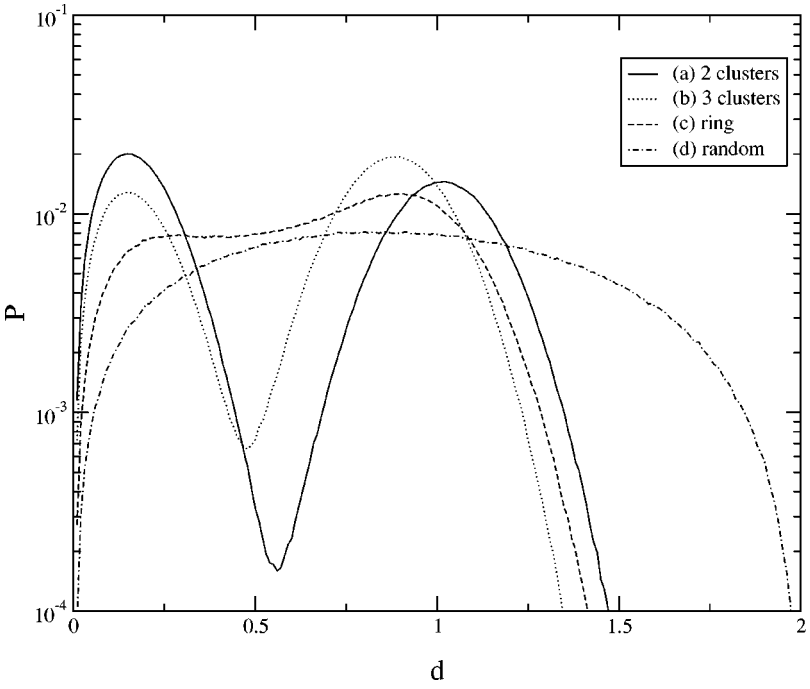

FIG. 6. Average of $P(d)$, the distance distribution, for different simulated spatial configurations. See text.

certain amount of particles in order to increase I. Near the ground state these ''free'' particles will eventually collapse to form a second cluster in order to decrease the potential energy ϕ. Due to the conservation of the center of mass, the position of the biggest cluster will be shifted from the center by a certain amount [see Fig. 5(b) at $\epsilon=-5$]. At low Ω one particle will be ejected, with increasing Ω the number of ejected particles raises and this process stops when two equal-size clusters are formed. This explains the discreteness of the peaks in ω (Fig. 4) and the increase of the ground state energy $\epsilon_g(\Omega)$, because the potential energy of a single cluster of size N is smaller than that of two well separated clusters. At high ($\Omega \gtrsim 12$) the system undergoes a phase transition from a gas phase to a collapse phase with two equal-size clusters close to the boundary. From one value of $\Omega=\Omega_1 > 12$ to another one $\Omega_2 > \Omega_1$, the whole entropy curve at fixed angular momentum is simply shifted along the energy axis, i.e., $S(\epsilon,\Omega_1) \approx S(\epsilon+[\Omega_2-\Omega_1]/N,\Omega_2)$. So the ground state energy $\epsilon_g(\Omega)$ at high Ω is almost on the line of equation $\epsilon_g+\Omega/N+\phi_g \approx 0$, where Ω/N and ϕ_g are the rotational energy and the potential energy of two clusters of size $N/2$ at radius $r=1$, respectively. This monotonic behavior has already been mentioned for all the thermodynamical variables S (Fig. 2), β (Fig. 3), ω (Fig. 4), etc.

As already mentioned ρ is only a function of r and it cannot be used to infer the angular distribution of the particles, i.e., there is not enough information to say if a peak in ρ at $r_0 \neq 0$ corresponds to one or many-cluster or to a uniform distribution of the particles (ring) lying on a circle of radius r_0. However at least at very low-energy a many cluster (more than two) configuration is very unlikely and will not contribute to the average values for reasons linked to the weight $W(\boldsymbol{r})=(1/\sqrt{I})\epsilon_r^{N-5/2}$. For simplicity let us assume that there is only one strong peak in ρ at $r=r_0 \neq 0$. Since the center of mass is fixed this cannot be the signature of a one-cluster system. At least two-clusters lying on a circle of radius r_0 are needed. All these n-cluster systems have the same rotational energy $\Omega/I=\Omega/Nr_0^2$, but their corresponding potential energy ϕ_n will differ. For example, with $\sigma=0.05$, $r_0=0.5$, and $N=24$ the ratio of potential energy is $\phi_2/\phi_3 \simeq 1.7$. So at low energy, the remaining energy ϵ_r corresponding to a two-cluster system will be much larger than the three-cluster one, leading to a *huge* difference in the weight $W(\boldsymbol{r})$. So at low energy and for $\Omega \neq 0$ the two-cluster case is dominant. At higher energies, the term $D(I,\phi)$ in Eq. (21) can compensate for the difference in the weight $W(\boldsymbol{r})$ and allow many-cluster configurations and eventually at high energy, a complete random configuration on the ring of radius r_0 will dominate the average mass distribution.

We can check this argument by studying another observable, for example, the normalized distance distribution $P(d)$, i.e., the density of probability that the distance between two given particles is d. To probe the information given by $P(d)$ we have estimated it for four simple mass distributions: (a) two-clusters, (b) three-clusters, (c) a ring, (d) a uniform random distribution. For (a), (b), and (c) the particles were put on a circle of radius $r_0=0.5$, and then randomly shifted several times (in order to give a spatial extension to these idealized initial configurations); finally the $N(N-1)/2$ distances are recorded for all realizations and averaged. Figure 6 shows the average of $P(d)$ over 1000 realizations. Note that the density distribution $\rho(r)$ is by construction exactly the same for the first three cases, i.e., strongly peaked at r_0 with a width of about 0.5. The latter value depends on the shift one applies on the initial idealized spatial configurations.

As one can see in Fig. 6, although the density distribution is the same for (a), (b), and (c), $P(d)$ gives some new insight on the mass distribution.

(a) There are two peaks, one centered at small d, which corresponds to a clusterization, and another one at $r \simeq 1 = 2r_0$; this is exactly the distance between the two clusters

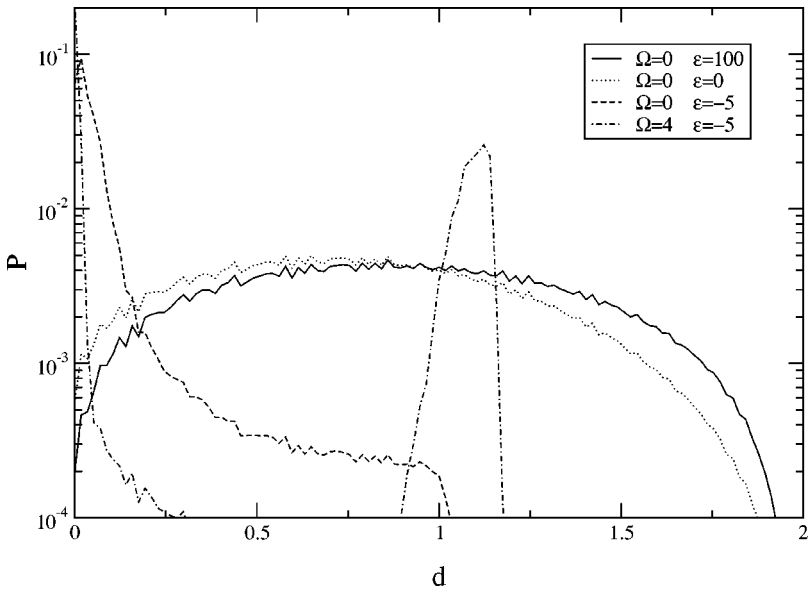

FIG. 7. Distance distribution $P(d)$ for the gravitational case for different values of (ϵ,Ω). At high energy $P(d)$ corresponds to a random distribution (see Fig. 6). For $\Omega=0$ and at low energy, $P(d)$ has one peak at $d\approx 0$; almost all particles are very close to each other and there is a single-cluster collapse phase. For $\Omega\neq 0$ there are two peaks at low energy: one at very small d, which is a sign of clusterization, and another peak at large d, which signals multiple clusterization; in fact there are two clusters (see text).

(more precisely between their center of mass). The area under the small d peak is similar to that under the large d peak. Indeed the number of short distance pairs and the number of pairs with $d\simeq 1$ are both about $N^2/4$. Moreover the widths of the first and second peaks are (as expected) ~ 0.5 and $\sim 1 = 2\times 0.5$ respectively.

(b) There are again two peaks, one at small d and another at $d\simeq 0.8<1$, and their respective widths are similar to those in (a). The large d is compatible with the length of one side of the equilateral triangle on top of which the three-cluster mass distributions were built. This time the area under the large d peak is larger than that under the short d peak, since the number of short distance pairs is about $N^2/6$ whereas the number of pairs with $d\simeq 0.8$ is $N^2/3$.

(c) For the ring case a trace of the two peaks still exists but they are not well separated because a lot of intermediate distances are compatible with this model.

(d) When the particles are uniformly distributed $P(d)$ has a binomial-like shape.

We have also estimated $P(d)$ for our gravitational system, as shown in Fig 7. At high energy, $P(d)$ corresponds to the randomly distributed case (see Fig. 6). At low energy with $\Omega=0$, $P(d)$ has only one peak at $d=0$, this corresponds clearly to a single-cluster case surrounded by some gas. For $\Omega\neq 0$ and at low energy (in Fig. 7, $\epsilon=-5$ and $\Omega=4$), there are two well separated peaks, one at small $d_0=0$ and the other at $d_1\simeq 1.1$. The peaks imply the presence of at least two clusters, however the fact that the widths of the peaks are small excludes a large number of clusters and even more so the ring case (see Fig. 6). Now we can combine these informations with those obtained from $\rho(r)$ (see Fig. 5). For $\epsilon=-5$ and $\Omega=4$, ρ has two peaks at $r_1\simeq 0.15$ and $r_2\simeq 1$. All in all, this means that there are, on an average, mean, two clusters rotating around the center of mass. The distance between these clusters is $r_1+r_2\simeq d_1\simeq 1.15$. Due to the fixed center of mass their mass ratio is $m_2/m_1=r_1/r_2\simeq 0.15$. Since we know the total mass $m_1+m_2=20$ we get $m_1\simeq 17$ and $m_2\simeq 3$.

The distance distribution can be of great help to identify the mass distributions at low energies. However in the transition region since there is a superposition of different types of mass distributions, the knowledge ρ and $P(d)$ is not sufficient and, therefore, of no help if we want to study, for example, the ''fractality'' of the mass distribution as has been discussed in other self-gravitating systems [52–54] (not mentioning the fact that the actual number of particles in the presented numerical applications is too small), and further work is needed to get a more detailed picture.

At very low energy, near the ground state at least one of the clusters (the smallest) is very close to the boundary. There the assumption of a small evaporation rate made in Sec. I does not hold.

C. Phase diagram

In Fig. 8 we have plotted $\mathrm{sgn}[\lambda_1(\epsilon,l)]$ as defined in Sec. II B. This plot can be taken as the phase diagram of the self-gravitating system at fixed ϵ and l. The white regions correspond to pure phases ($\lambda_1<0$). At high energy there is a homogeneous gas phase and at low energy there are several pure collapse phases with one ($\Omega=0$) or two ($\Omega\neq 0$) clusters. The different two-cluster phases are characterized by the relative size of their clusters (see Sec. III B). These regions are separated by a first order phase transition region where $\lambda_1>0$ (gray in Fig. 8). There is even a region (dark gray) where the entropy S is a convex function of ϵ and l; i.e., all the eigenvalues of H_S are positive ($\lambda_1>0$ and $D_S>0$). This region is quite stable with respect to the number of particles (at least for $N<100$). Its specific surface increases slightly with the number of particles N. The orientation of $\mathbf{v}_1$, the eigenvector associated with λ_1, is not yet known in detail for all (ϵ,l). However, we can already state that at high energy $\mathbf{v}_1$ is almost parallel to the energy axes and should be parallel to the ground state at very low energy. The overall structure of the collapse phases matches that of the angular velocity ω (see Fig. 4). Roughly, the peaks in ω correspond to pure

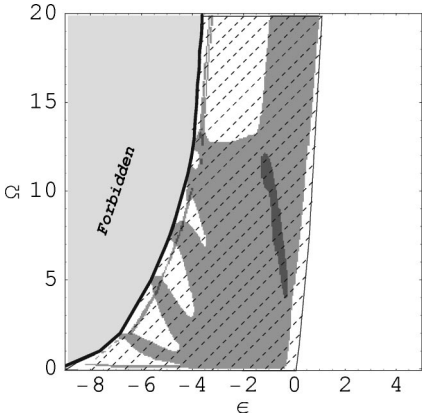

FIG. 8. Sign of the largest eigenvalue λ_1 of H_S, the Hessian matrix of S, as defined in Sec. II B. The white regions correspond to $\lambda_1<0$. These are pure phase regions. The gray region corresponds to $\lambda_1>0$ and $\lambda_2<0$ and the dark gray ones also to $\lambda_1>0$ but with $\lambda_2>0$. λ_2 is the second eigenvalue of H_S. $\lambda_1>0$ defines first order phase transition regions (see text). Points in G (the region filled with dashed lines) correspond to *local* maxima (minima) of $f(X,X_0)=-x_0X+S(X)$ if $\lambda_1(X_0)<0$ $[\lambda_1(X_0)>0]$, see Eq. (25). Points outside G correspond to the *global* maxima of $f(X,X_0)$. There is a one-to-one mapping between the microcanonical and the canonical ensembles only outside the G region (see text). S is not defined in the *forbidden* region, here in light gray. Note that (a) the points at $\Omega=0$ and low energies $\epsilon<-7$ are not included in G, (b) the high energy limit of G is known only approximately.

phases while the valleys between these peaks belong to the first order phase transition region.

As already mentioned, unlike in the model presented by Laliena in [26], there is no critical angular momentum L_c above which the first order phase transition vanishes giving rise to a second order phase transition at L_c. Nevertheless this does not exclude second order phase transition (critical point) at all. They are defined in the microcanonical ensemble by (i) $\lambda_1=0$, (ii) $\nabla\lambda_1\cdot\mathbf{v}_1=0$ (see Sec II B). In Fig. 9 (just like in Fig. 8) regions where $\lambda_1<0(>0)$ are in white (gray). The condition (i) is simply achieved at the border between the gray and the white regions [λ_1 is a continuous function over the whole parametric space (ϵ,l)]. The thick lines on Fig. 9 correspond to condition (ii). Second order phase transitions are located at the crossing points of the thick lines and the borders. One immediately sees that there are several critical points. However there are not all of (astro-) physical interest since most of them are close to the ground state line or at very high angular momentum where the small evaporation rate assumption is not valid. Nevertheless there are two points, one at $(\epsilon,\Omega)\approx(-0.5,1)$ and another one at $(\epsilon,\Omega)\approx(-0,4)$, where this assumption is valid and, therefore, they deserve further investigations, especially regarding their corresponding mass distributions.

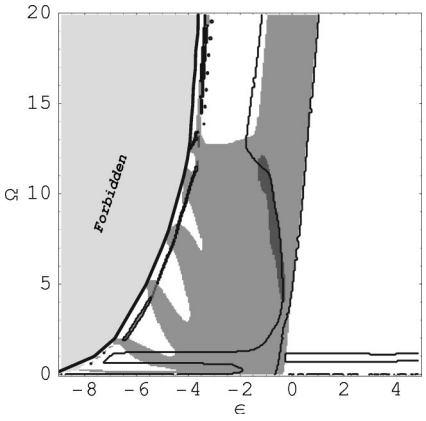

FIG. 9. Locus of second order phase transitions (see text).

D. Loss of information in canonical ensembles

Once one defines the generalized microcanonical ensemble (ME), it is straightforward to introduce and study the system in its conjugate ensemble, the generalized canonical ensemble (CE). Note that ''generalized'' means in CE ''as a function of all the intensive variables'' and, in ME ''as a function of all extensive parameters.'' There are mainly two reasons for studying a system in CE instead of in ME

(1) Performing the computations in CE is in most cases much easier than in ME. Here CE can be seen as a trick [55]. However there is *a priori* no reason for the results to be equivalent. Indeed the strict equivalence of the ensemble is only achieved at the thermodynamical limit except in the first order phase transition regions [35,34,45]. In a weaker sense, needed for ''Small'' systems, ME and CE can only be equivalent when $\lambda_1(X)<0$ and far from any first order phase transition regions (see below). Moreover recent progress in computer performance now enables one to perform numerical experiments within the ME for increasingly complex systems.

(2) The studied system is not isolated but is in contact with a ''heat bath'' and can exchange amounts of X with it. Then, obviously ME does not provide a suitable description, and CE might be eligible. Here CE describes a *different* physical system than that in ME. At the thermodynamical limit (if it exists) the ensembles are again equivalent except at first order phase transitions. However, the CE description is valid only if the Hamiltonian of interaction, $\mathcal{H}_{int}$, is small compared to those of the system, $\mathcal{H}_{sys}$, and the heat bath, $\mathcal{H}_{hb}$. This condition is usually fulfilled at the thermodynamical limit (if it exists), but for ''Small'' systems the Hamiltonian of interaction, $\mathcal{H}_{int}$, can hardly be small at least compared to $\mathcal{H}_{sys}$ and this can lead to dramatic effects [56,57]. In this case a better description would be the ME of the system, its heat bath, and their interactions.

For now on we consider in this paper the cases when CE is used as a mathematical trick, and we focus on the amount of information lost from ME to CE.

The link between ME and CE is given by the Laplace transform (using the notations introduced in Sec. II B)

$$\mathcal{Z}(x)=\int_0^\infty dX e^{-Xx+S(X)}, \tag{25}$$

where $\mathcal{Z}$ is the partition sum of the CE, $x=\{x^1,\ldots,x^{\mathcal{M}}\}$ are the intensive variables associated with X and defined by

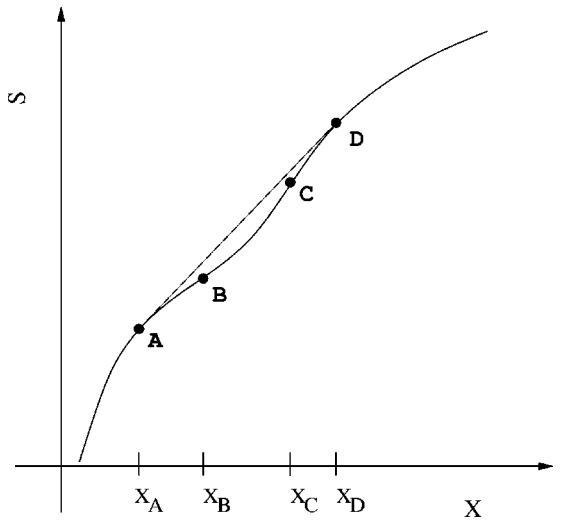

FIG. 10. Schematic entropy curve S as a function of one extensive parameter X (solid line) and the Maxwell line (dashed line). A and D are the end points of the Maxwell construction. At B and C the largest curvature vanishes, i.e., $\lambda_1=0$. All the points below the Maxwell line do not correspond to a global maximum in the Laplace transform, Eq. (25). This includes points where $\lambda_1=\partial^2 S/\partial X^2>0$, but also points where the entropy is concave, for $X\in[X_A,X_B]$ and $X\in[X_A,X_B]$, $\lambda_1(X)<0$.

$$x^i \equiv \frac{\partial S}{\partial X^i} \tag{26}$$

for $i=1,\ldots,\mathcal{M}$. The ME at X_0 is equivalent to the CE at $x_0=x(X_0)$ if the integrand in Eq. (25), $e^{f(X,x_0)}$, and therefore $f(X,x_0)=-Xx_0+S(X)$ has a *global maximum* at X_0 [44]. This condition is violated when $\lambda_1(X_0)>0$ (this is the basic idea behind the definition of phase transitions in "small" systems, see [34]). So in practice all informations are contained in points where $\lambda_1>0$ are lost after the Laplace transform (25) in CE.

Now we are left with the points X_0 characterized by $\lambda_1(X_0)<0$. This relation implies only that $f(X,x_0)$ has a *local* maximum at X_0 but not that it is a *global* one; $\lambda_1<0$ is a necessary but not sufficient condition. In Fig. 10 we have illustrated this point with a trivial one-dimensional example. All the points below the Maxwell line do not correspond to global maxima and their information content is smeared out and, in practice, lost in CE.

From the last remark we see that a way to check if a point corresponds to a global maximum in Eq. (25) is to study what would be a generalization of the Maxwell line in $\mathcal{M}>1$ dimensions. Work is in progress in this direction and the results will be presented elsewhere, but we can already state that this task is, to some extent, similar to that of building the *convex hull* of a set of points in $\mathcal{M}$ dimensions, or more specifically the convex hull of the entropy S.

However, if one needs qualitative results, in two dimensions the task can be rather easily solved in another way. Let us define $p(X,X_0)$ as the tangent plane to $S(X)$ at X_0; its equation is $p(X,X_0)=-Xx_0+S(X_0)+X_0x_0$. If $f(X,x_0)$ has a global maximum at X_0 then

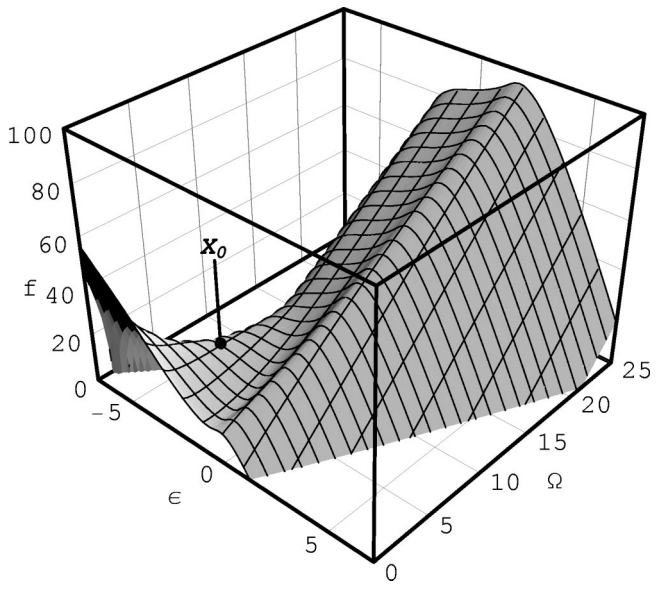

FIG. 11. $f(\epsilon,\Omega,\beta_0,\gamma_0)=-\epsilon\beta_0-\Omega\beta_0\gamma_0+S(\epsilon,\Omega)-K$ as a function of ϵ and Ω, where K is an arbitrary constant, $\beta_0=\beta(\epsilon_0,\Omega_0)$, $\Omega_0=\Omega(\epsilon_0,\Omega_0)$, $X_0=(\epsilon_0,\Omega_0)=(-3,5)\Rightarrow(\Omega_0,\gamma_0)\approx(27.9,-0.196)$. The mesh lines are at constant ϵ or constant Ω. As expected f has a saddle point at $X_0\approx(\beta_0,\gamma_0)$ since $m(X_0)>0$ and $D_S(X_0)<0$ (see text and Fig. 8). f has a global maximum at $\Omega=0$ and $\epsilon\approx-7$, but one sees that it is a monotonically increasing function for increasing Ω and $\epsilon(\Omega)\approx\epsilon_g(\Omega)+2$. Therefore the integral in Eq. (25) *diverges* and the $(\beta,\gamma\beta)$ ensemble is *not defined* for (β_0,γ_0).

$$p(X,X_0)>S(X) \tag{27}$$

for all $X\neq X_0$ and $p(X_0,X_0)=S(X_0)$ by definition.

In the case of the gravitational model presented here $X=\{\epsilon,\Omega\}$ and $x=\{\beta,\gamma\beta\}$ (GBE). Now if one inspects the entropy surface $S(X)$ (see Fig. 2) it is clear that condition (27) is not satisfied for all the points in the region filled with dashed lines (G) in Fig. 8. This is due to the concavity of the energy ground state $\epsilon_g(\Omega)$ (see Sec. III A). G includes all the two-cluster collapsed phases and the first and second order phase transitions (except for $\omega=\Omega=\gamma=0$). All the information contained in G is smeared out through the Laplace transform (25) in GBE and is, in practice, lost.

The fact that GBE misses all the two-cluster collapse phases would be already enough to disqualify it as being a good approximation (mathematical trick) of the ME. But, furthermore, if one studies more carefully $f(X,x_0)$, $X_0\in G$; one will notice that (a) there is one local maximum at $\Omega=0$ and (b) there is no maximum for high Ω: in the direction of increasing Ω at low energy, $f(X,x_0)$ is a never ending increasing function, i.e., $f(X,x_0)$ has *no global maximum* for $X_0\in G$ (see Fig. 11). Therefore the integral in Eq. (25) *diverges* for all x_0, $X_0\in G$. In other words the GBE, in our model, is *not defined* for high β and $\gamma\neq0$ $(\omega\neq0)$.

One could argue that GBE is not the correct CE for this system. I.e., one should rather fix the conjugates of ϵ and l, as the inverse temperature β and the angular velocity ω, respectively. By following the same path as for GBE one can show that contrary to GBE, the standard canonical ensemble

is defined everywhere. However, one can also show that no point $X_0=(\epsilon_0,l_0)$ in the region where $\epsilon\lesssim 0$ and $l\lesssim 5$ (it includes *G*, see Fig. 8) corresponds to a global maximum of the function $f(\epsilon,l,\beta_0,\omega_0)=-\epsilon\beta_0-l\beta_0\omega_0+S(\epsilon,l)$. This implies that all the asymmetric pure phases are overlooked by CE. In other words they do not correspond to global minima of the canonical free energy. This is also the case for the two critical regions at relatively high energies.

These examples show how dramatic can the information loss be if one studies an isolated system as a function of intensive parameters.

IV. SUMMARY AND DISCUSSION

A. Summary

The aim of this paper is to present the results of a study of a self-gravitating system of *N* classical particles on a disk of radius *R* for which two extensive variables, namely, total energy *E* and total angular momentum *L* are fixed. The microcanonical entropy *S* can be written as the logarithm of an integral over the spatial configurations (3) and (5). The conservation of *L* implies that the mean value of the linear momentum $\boldsymbol{p}$ of a particle at a radial distance *r* is proportional to *L* and *r*, Eq. (13); on an average the system rotates like a solid body, i.e., the mean angular velocity of a particle does not depend on its position (17). The dispersion of $\boldsymbol{p}$ is broader than what it would be if *L* is not be conserved and depends on the radial position (18). In order to integrate e^S we write it as the folding product of a ''background'' function *D* and the weight associated with the remaining energy (21). Once a numerical estimate of *D* is obtained, *S* and its derivatives, such as the inverse temperature β, can be computed. The entropy surface shows an intruder in the energy direction, which signals a first order phase transition with negative specific heat capacity (Figs. 2 and 3). Contrary to another model [26] there is no critical value of *L* above which this transition is no longer present. At high energy the angular velocity ω is a simple increasing function of *L* [Eq. (8) and Fig. 4], but at low energy, near the ground states, the relation between *L* and ω becomes nontrivial. All these peculiarities can be understood if we study the mass distribution. We use two observables: the density of mass, ρ, as a function of the radial distance and $P(d)$, the density probability that the distance between two particles is *d*. At fixed *L* and at high energy the particles are randomly distributed over the disk (gas phase). If the energy decreases, below some threshold the system undergoes a phase transition of first order to a collapse phase. If $L=0$ there is a single cluster at the center of mass, if $L\neq 0$ then there are two clusters rotating around the center of mass. Their relative mass m_1/m_2 with $m_1>m_2$ is very large for low *L*, it decreases as *L* raises and eventually becomes 1 for *L* larger than a certain threshold. Clearly these two clusters phases were not reported in previous work because of the usual *a priori* assumption of rotational symmetry.

Phase transitions (and phases) can be defined unambiguously in the microcanonical ensemble as a function of the *local* topology of *S*. If all eigenvalues of H_S, the Hessian matrix of *S*, are negative then the system is in a pure phase. If (at least) one eigenvalue is positive, say λ_1, then there is a first order phase transition in the direction of $\mathbf{v}_1$, the eigenvector associated with λ_1. A critical behavior occurs when one (or many) eigenvalue vanishes on at least a second order region (if $\lambda_1=0$, $\boldsymbol{\nabla}_{\mathbf{v}_1}\lambda_1=0$). Note that one can find positive, negative, and zero eigenvalues at the same point in the parameter space. Using these criteria, we can draw a phase diagram of the gravitational system (Fig. 8) at fixed *E* and *L*: at high energy there is a pure gas phase; at low energy there are several pure collapse phases, there is one cluster at $L=0$, and there are two clusters for $L\neq 0$, these phases are separated by first order phase transition regions. There are also several second order phase transitions, two of them are located at relatively high energies ($E\approx 0$) and, therefore, may be of astrophysical importance.

Studying an isolated system using the CE can be very misleading, since there is a massive loss of information from the correct ME description to that of the CE (if there are phase transitions in ME). In fact for the gravitational model, *CE cannot be sensitive to the asymmetric two-cluster phases and all the phase transitions*, and the γ-β ensemble (GBE) as defined in Sec. III D *is not defined for some values of the intensive parameters that exist in ME.*

B. Discussion

Of course we have just presented an *equilibrium statistical* model that may help to understand the physics of globular clusters or collapsing molecular clouds, but the results should be interpreted with caution especially in the case of star formation. A lot of ''ingredients'' are missing in order to have a complete picture of the formation of multiple stars systems and planetary systems, for instance, the magnetic field [58,59] or the presence of vortices [60].

Phases and phase transitions can be well defined in the ME without invoking the thermodynamical limit by probing the curvature of the entropy surface. There still exist open problems. One of them is the scaling of a first order transition: in Fig. 10, in a canonical sense the phase transition occurs from X_A to X_D (if *X* is the energy *E* then X_D-X_A is the transition latent heat), but if one uses the ME definition the transition occurs only from X_B to X_C. At the thermodynamical limit, if it exists, such discrepancy should disappear. In another context (a model of a first order liquid gas transition of finite-size sodium clusters) we could show that $(X_C-X_B)/(X_D-X_A)\rightarrow 1$ when the system size goes to infinity [44].

The ME definition of phase transitions offers a richer view of physical systems and phase transitions. Again in Fig. 10, CE is not sensitive to everything that could happen under the Maxwell line: there is always one transition. On the contrary, in ME there could be many phase transitions between X_A and X_D. For example, if there is a small positive curvature bump between X_B and X_C there would be two transitions in the microcanonical sense but still one in the canonical sense.

ACKNOWLEDGMENTS

We are grateful to V. Laliena, D. Valls-Gabaud, and P.-H. Chavanis for useful comments and criticisms. We also thank E. Votyakov for discussions and technical help.

APPENDIX

Let us compute $\langle \boldsymbol{p}_k \rangle_{\boldsymbol{q}_k}$ the average momentum of particle k at fixed position (for simplicity we will set $k=1$). The α component of $\langle \boldsymbol{p}_1 \rangle_{\boldsymbol{q}_1}$ is

$$\langle p_1^\alpha \rangle_{\boldsymbol{q}_1} = \frac{\int \left(\prod_i d\boldsymbol{p}_i \prod_{i=2}^N d\boldsymbol{q}_i \right) p_1^\alpha \delta(E-\mathcal{H}) \delta^{(2)}\left(\sum_i \boldsymbol{p}_i \right) \delta\left(\sum_i \boldsymbol{q}_i \times \boldsymbol{p}_i - L \right) \delta^{(2)}\left(\sum_i \boldsymbol{q}_i \right)}{\int \left(\prod_i d\boldsymbol{p}_i \prod_{i=2}^N d\boldsymbol{q}_i \right) \delta(E-\mathcal{H}) \delta^{(2)}\left(\sum_i \boldsymbol{p}_i \right) \delta\left(\sum_i \boldsymbol{q}_i \times \boldsymbol{p}_i - L \right) \delta^{(2)}\left(\sum_i \boldsymbol{q}_i \right)} = \frac{\int \left(\prod_{i=2}^N d\boldsymbol{q}_i \right) \mathcal{P}_1^\alpha \delta^{(2)}\left(\sum_i \boldsymbol{q}_i \right)}{\int \left(\prod_{i=2}^N d\boldsymbol{q}_i \right) W(\mathbf{r}) \delta^{(2)}\left(\sum_i \boldsymbol{q}_i \right)}, \tag{A1}$$

where $\mathcal{P}_1^\alpha = \int (\Pi_i d\boldsymbol{p}_i) p_1^\alpha \delta(E-\mathcal{H}) \delta^{(2)}(\Sigma_i \boldsymbol{p}_i) \delta(\Sigma_i \boldsymbol{q}_i \times \boldsymbol{p}_i - L)$, and $W(\mathbf{r})$ is the microcanonical weight at a fixed spatial configuration $\mathbf{r}$, its value is $W(E,L,\mathbf{r}) = \mathcal{C}(1/\sqrt{I}) E_r^{N-5/2}$ [see Eq. (5)]. The outline of the derivation of $\mathcal{P}_1^\alpha$ is the same as in [26] for W, and we get after some algebra

$$\mathcal{P}_1^\alpha = \mathcal{C} L m_1 I^{-3/2} \sum_{\delta=1}^2 q_1^\delta \boldsymbol{\epsilon}_{\delta\alpha} E_r^{N-5/2}, \tag{A2}$$

where $\boldsymbol{\epsilon}$ is the antisymmetric tensor of rank 2. Using Eq. (A2) in Eq. (A1) we get finally

$$\langle p_1^\alpha \rangle_{\boldsymbol{q}_1} = \frac{\int \left(\prod_{i=2}^N d\boldsymbol{q}_i \right) \mathcal{C} L m_1 I^{-3/2} \sum_{\delta=1}^2 q_1^\delta \boldsymbol{\epsilon}_{\delta\alpha} E_r^{N-5/2} \delta^{(2)}\left(\sum_i \boldsymbol{q}_i \right)}{\int \left(\prod_{i=2}^N d\boldsymbol{q}_i \right) I^{-1/2} \sum_{\delta=1}^2 q_1^\delta \boldsymbol{\epsilon}_{\delta\alpha} E_r^{N-5/2} \delta^{(2)}\left(\sum_i \boldsymbol{q}_i \right)} = L m_1 \langle I^{-1} \rangle_{\mathbf{q}_1} \sum_\delta q_1^\delta \boldsymbol{\epsilon}_{\delta\alpha}. \tag{A3}$$

Finally,

$$\langle \boldsymbol{p}_1 \rangle_{\boldsymbol{q}_1} = L m_1 \langle I^{-1} \rangle_{\mathbf{q}_1} \sum_{\delta,\alpha} q_1^\delta \boldsymbol{\epsilon}_{\delta\alpha} \hat{\mathbf{e}}_\alpha, \tag{A4}$$

where $\hat{\mathbf{e}}_\alpha$ is the α component's unit vector.

$\langle \boldsymbol{p}_k^2 \rangle_{\boldsymbol{q}_k}$ can be derived in a similar way and we get

$$\langle \boldsymbol{p}_k^2 \rangle_{\boldsymbol{q}_k} = \frac{2m_k}{(N-5/2)\langle E r^{-1} \rangle_{\boldsymbol{q}_k}} \left(1 - \frac{m_k}{M} \right) - \frac{m_k I_k}{I(N-5/2)\langle E r^{-1} \rangle_{\boldsymbol{q}_k}} + I_k L^2 m_k \langle I^{-2} \rangle_{\boldsymbol{q}_k}. \tag{A5}$$

[1] V. Antonov, Vestn. Leningr. Gros. Univ. **7**, 135 (1962).
[2] T. Padmanabhan, Phys. Rep. **188**, 285 (1990).
[3] D. Lynden-Bell, Mon. Not. R. Astron. Soc. **136**, 101 (1967).
[4] D. Lynden-Bell and R. Wood, Mon. Not. R. Astron. Soc. **138**, 495 (1968).
[5] P. Hertel and W. Thirring, Ann. Phys. (USA) **63**, 520 (1971).
[6] W. Thirring, Z. Phys. **235**, 339 (1970).
[7] W. C. Saslaw, *Gravitational Physics of Stellar and Galactic Systems* (Cambridge University Press, Cambridge, 1985).
[8] G. B. Lima Neto, D. Gerbal, and I. Márquez, Mon. Not. R. Astron. Soc. **309**, 481 (1999).
[9] A. R. Lima, P. M. C. de Oliveira, and T. J. P. Penna, J. Stat. Phys. **99**, 691 (2000).
[10] J. Binney and S. Tremaine, *Galactic Dynamics*, Princeton series in astrophysics (Princeton University Press, Princeton, NJ, 1987).
[11] C. Lagoute and P.-Y. Longaretti, Astron. Astrophys. **308**, 441 (1996).
[12] C. Lagoute and P.-Y. Longaretti, Astron. Astrophys. **308**, 453 (1996).
[13] G. Horwitz and J. Katz, Astrophys. J. **211**, 226 (1977).
[14] D. Lynden-Bell, e-print astro-ph/0007116.
[15] F. Combes, Celest. Mech. Dyn. Astron. **72**, 91 (1998).
[16] H. J. de Vega, N. Sánchez, and F. Combes, in *Fractal Structures and Scaling Laws in the Universe: Statistical Mechanics of the Self-Gravitating Gas*, edited by M. S. El Naschie and C. Castro, special issue of Chaos, Solitons Fractals **10**, 329 (1999).
[17] M. R. Bate, Astrophys. J. Lett. **518**, L95 (1998).
[18] R. I. Klein, R. T. Fisher, C. F. McKee, and J. K. Truelove, in *ASSL Vol. 240: Numerical Astrophysics*, edited by S. M. Miyama, K. Tomisaka, and T. Hanama (Kluwer Academic, Boston, MA, 1999).
[19] R. S. Klessen and A. Burkert, in *ASSL Vol. 263: New Horizons of Computational Science*, edited by T. Ebisuzaki and J.

Makino (Kluwer Academc, Boston, MA, 2001).
[20] A. Burkert and P. Bodenheimer, Mon. Not. R. Astron. Soc. **280**, 1190 (1996).
[21] A. P. Whitworth, N. F. A. S. Bhattal, and S.J. Watkins, Mon. Not. R. Astron. Soc. **283**, 1061 (1996).
[22] S. D. M. White, in *Gravitational Dynamics*, edited by E. T. R. Terlevich and O. Lahav (Cambridge University Press, Cambridge, 1996).
[23] P. J. Klinko and B. N. Miller, Phys. Rev. E **62**, 5783 (2000).
[24] In [23] the sum of the square of the angular momentum of the individual particles is fixed, whereas in the present paper the square of the *total* angular momentum is fixed. The latter quantity, contrary to the former, is, in our model, a constant of motion.
[25] D. M. Christodoulou and J. E. Tohline, Astrophys. J. **363**, 197 (1990).
[26] V. Laliena, Phys. Rev. E **59**, 4786 (1999).
[27] K. R. Yawn and B. N. Miller, Phys. Rev. E **56**, 2429 (1997).
[28] C. J. Reidl, Jr. and B. N. Miller, Phys. Rev. E **48**, 4250 (1993).
[29] J. Sommer-Larsen, H. Vedel, and U. Hellsten, Astrophys. J. **500**, 610 (1997).
[30] E. Follana and V. Laliena, Phys. Rev. E **61**, 6270 (2000).
[31] A. B. Romeo, Astron. Astrophys. **324**, 523 (1997).
[32] P. H. Chavanis and J. Sommeria, Mon. Not. R. Astron. Soc. **296**, 569 (1998).
[33] T. D. Lee and C.N. Yang, Phys. Rev. **87**, 410 (1952).
[34] D. H. E. Gross and E. Votyakov, Eur. Phys. J. B **15**, 115 (2000).
[35] D. H. E. Gross, *Microcanonical Thermodynamics: Phase Transitions in "Small" Systems*, Lecture Notes in Physics Vol. 66 (World Scientific, Singapore, 2001).
[36] H. C. Plummer, Mon. Not. R. Astron. Soc. **71**, 460 (1911).
[37] G. Yepes, in *From Quantum Fluctuations to Cosmological Structures*, ASP Conferences Vol. 126, edited by D. Valls-Gabaud, M. Hendry, P. Molaro, and K. Chamcham (Astronomical Society of the Pacific, Provo, UT, 1997), p. 279.
[38] F. Calvo and P. Labastie, Eur. Phys. J. D **3**, 229 (1998).
[39] B. Diu, C. Guthmann, D. Lederer, and B. Roulet, *Physique Statistique* (Hermann, Paris, 1989).
[40] R. E. Kunz and R. S. Berry, Phys. Rev. E **49**, 1895 (1994).
[41] D. H. E. Gross and P. A. Hervieux, Z. Phys. D: At., Mol. Clusters **33**, 295 (1995).
[42] H. A. Posch, H. Narnhofer, and W. Thirring, Phys. Rev. A **42**, 1880 (1990).
[43] D. H. E. Gross, M. E. Madjet, and O. Schapiro, Z. Phys. D: At., Mol. Clusters **39**, 75 (1997).
[44] O. Fliegans, Ph.D. thesis, Freie Universität Berlin, 2001; http://www.diss.fu-berlin.de/2001/93/gesamt.pdf
[45] L. Landau and E. Lifchitz, in *Physique Statistique* (Mir-Ellipses, Moskow, 1994), Chap. II.26.
[46] A. Torcini and M. Antoni, Phys. Rev. E **59**, 2746 (1999).
[47] J. Lee, Phys. Rev. Lett. **71**, 211 (1993).
[48] B. A. Berg, U. Hansmann, and T. Neuhaus, Phys. Rev. B **47**, 497 (1993).
[49] A. M. Ferrenberg and R. H. Swendsen, Phys. Rev. Lett. **63**, 1195 (1989).
[50] G. R. Smith, Ph.D. thesis, University of Edinburgh, 1996, http://indigo1.biop.ox.ac.uk/graham/graham.html
[51] A set $\mathcal{C}$ of $\mathbb{R}^n$ is said to be *convex* if for any couple of points M and N $(M \neq N)$ of $\mathcal{C}$, the segment $[M,N]$ is in $\mathcal{C}$.
[52] H. J. de Vega and N. Sánchez, Phys. Lett. B **490**, 180 (2000).
[53] Y. Sota, O. Iguchi, M. Morikawa, T. Tatekawa, and K. Maeda, e-print astro-ph/0009412.
[54] B. Semelin, Ph.D. thesis, Université Paris VI, 1999.
[55] P. Ehrenfest and T. Ehrenfest, *The Conceptual Foundation of the Statistical Approach in Mechanics* (Cornell University Press, Ithaca, NY, 1959), pp. 20–22.
[56] K. Sato, K. Sekimoto, T. Hondou, and F. Takagi, e-print cond-mat/0008393.
[57] K. Sekimoto, F. Takagi, and T. Hondou, Phys. Rev. E **62**, 7759 (2000).
[58] A. Hujeirat, P. Myers, M. Camenzind, and A. Burkert, New Astron. **4**, 601 (2000).
[59] D. Galli, F. H. Shu, G. Laughlin, and S. Lizano, in *Stellar Clusters and Associations*, edited by T. Montmerle and P. André of ASP Conference Series Vol. 198 (ASP, Provo, UT 2000).
[60] P.-H. Chavanis, Astron. Astrophys. **356**, 1089 (2000).